2018 International Conference on Unmanned Aircraft Systems (ICUAS)
Dallas, TX, USA, June 12-15, 2018

Aerodynamic modeling of the Skywalker X8 Fixed-Wing Unmanned Aerial Vehicle

Kristofer Gryte, Richard Hann, Mushfiqul Alam, Jan Roháč, Tor Arne Johansen and Thor I. Fossen

***Abstract*— With advanced control, estimation and simulation requirements in unmanned aerial systems comes the need for sophisticated aerodynamic models. This paper reviews two common means for establishing such models; numerical design tools and wind tunnel testing, by presenting strengths and potential problems, in a "lessons learned"-manner. As a case study throughout the paper, a six degrees-of-freedom aerodynamic model of the Skywalker X8 fixed-wing unmanned aerial vehicle is presented.**

I. Introduction

The use of mathematical models to describe a fixed-wing aircraft's motion is a well known field. There are many reasons why a mathematical description of the aircraft motion is useful. First and foremost, it can be used in the design process of the aircraft, by considering how different design changes affect the performance. Another important use for an accurate model is simulation of flight conditions, which provides vital aiding for both pilots and control engineers, by saving time and money spent in initial training and control system testing. However, the applicability of the tests are limited by the accuracy of the model. A mathematical description of an unmanned aerial vehicle (UAV) is also crucial in model based control strategies. One example is model predictive control (MPC), where the model is used to minimize the control input needed to achieve the control objective, by predicting the response of the UAV. See for example [1], where MPC is used in deep stall landing. Similarly, model based estimation relies on a UAV model to propagate the estimates forward in time. See e.g. [2], where aerodynamic models are used in estimating the angle-of-attack and side-slip-angle of a UAV. Development of an aerodynamic model requires intimate knowledge of aerodynamics, in planing the wind tunnel tests and in analyzing the results, as well as knowledge in regression analysis, due to the large amounts of data produced by the tests.

One important tool in creating an aerodynamic model of a flying object is wind tunnel testing. Wind tunnels cause the air to move, instead of the flying object, so that the characteristics of how the flying object is affected by the air can be studied more easily. A problem with wind tunnel measurements, as with any measurement, is measurement errors. In the context of mathematical modeling, the objective of wind tunnel testing is to find the model, consisting of a structure and a set of parameters, that best describe the measured resulting aerodynamic forces and moments, given the measured characteristics of the flow and the forces and moments on aircraft[3], [4]. One possibility in identifying the parameters of the underlying aerodynamic model is through regression analysis, such as the least squares method.

Another option for creating an aerodynamic model is to perform system identification on data from flight tests. This refers to the process of designing appropriate control inputs to excite the system, measuring the response, and determine the type of model, and fitting the data to it. The advantages of this method is its close resemblance of real flight; any motion experienced during flight can, in theory, be modeled. Attitude, velocities, accelerations and airspeed are estimated using standard UAV avionics, and can be used in the identification. The main challenges with identification from flight tests are disturbances and noise. As opposed to wind tunnel experiments, flight testing is not performed in a controlled environment, and will be affected by external disturbances such as wind. Wind is particularly problematic for slow flying UAVs, since the wind velocity easily becomes large compared to the airspeed of the UAV. The uncertainty in the estimation of the state of the UAV will affect the accuracy of the system identification. A further challenge is to achieve sufficient excitation of the UAV. Finally, since many aerodynamic effects are dependent on the angle-of-attack or the side-slip-angle, they should be measured, if seeking a model of the aerodynamic coefficients in the wind frame. Unfortunately, sensors that are both capable of measuring these quantities, and are small and light-weight enough to fit in a UAV payload, are expensive.

In recent decades, numerical models have been developed to aid aircraft design and wind tunnel testing. Numerical design can reduce the number of tests needed to run in a wind tunnel, and its associated cost. There are two main types of numerical models currently used. The first type, computational fluid dynamics (CFD), is simulating the entire flow field around the aircraft, in either 2D or 3D, by solving the governing Navier-Stokes equations. CFD simulations are computationally expensive, and require experience, careful tuning, and time to set up [5]. In contrast, the so called panel methods use semi-empirical equations to predict the velocity

This work was partially supported by the EEA/Norway grant No. NF-CZ07-ICP-3-2082015 supported by the Ministry of Education, Youth and Sports of the Czech Republic and named Enhanced Navigation Algorithms in Joint Research and Education, partially by Norwegian Research Council (project no. 223254) through the NTNU Centre of Autonomous Marine Operations and Systems (NTNU AMOS) at the Norwegian University of Science and Technology, and partially by CIRFA grant number 237906.

[1] K. Gryte, R. Hann, T.A. Johansen and T.I. Fossen are with the Centre of Autonomous Marine Operations and Systems (NTNU AMOS), Department of Engineering Cybernetics, at the Norwegian University of Science and Technology, Trondheim, Norway

[2] M. Alam and J. Roháč are with the Czech Techincal University, Prague, Czech Republic

Corresponding author: kristoffer.gryte@ntnu.no

distribution along the surface of an airfoil, without resolving the flow field around it. These tools have low computational requirements and are easier to set up. They are by design limited to 2D calculations, although some model extensions also attempt to simulate 3D conditions with comparatively less accurate results. Examples of programs based on these methods are XFOIL [6], Surfaces Aircraft Design [7] and XFLR5 [8]. The latter is based on XFOIL and extends the model for 3D applications using lifiting line theory (LLT) and vortex lattice method (VLM), and is generally most accurate for thin lifting surfaces at small angles of attack. See also [9] for an extensive list of available software for aerodynamics and aircraft design, and [10] for a good introduction to panel methods.

However, all numerical models are approximations, and often the solution must be calibrated with the use of physical data from a wind tunnel. Thus it is reasonable, and important, to determine how realistic the data from the numerical software is, by relating it to experimental data [11].

In this paper, both the Vortex Lattice Method (VLM) of XFLR5 and wind tunnel data are used to create an aerodynamic model of a fixed-wing UAV. The stability coefficients are not measured in the wind tunnel, due to time restrictions and equipment limitations, and are therefore solely based on the XFLR5 analysis. For this reason it is important to assess the quality of the XFLR5 data, by comparing the static coefficients of XFLR5 with the wind tunnel data.

There exists several aircraft models that are available to the general public. Of the more notable are the NASA General Transportation Model (GTM) [12], NASAs large envelope F-16 model[13], [14], and the SIG Rascal 110 model [15] which is the standard fixed-wing model for ArduPlane Software-in-the-loop simulations with JSBSim[16]. Reference [17] includes a model of the Zagi flying wing UAV, based on aerodynamic modeling in DARCorp Advanced Aircraft Analysis program[18], verified by wind tunnel testing. The Zagi model is also given in [19], along with a model of an Aerosonde UAV.

The fixed-wing UAV considered in this paper is the Skywalker X8, produced by Skywalker Technology Co. Ltd. Its flying wing configuration gives a large payload area compared to the size of the UAV, and makes disassembly for transportation easier compared to conventional, tailed fixed-wing UAVs. These characteristics, in combination with its durability, low price point and availability, has lead the X8 to become very popular within the first person view (FPV) community, which was its original design purpose, and later also within various research facilities, which is the primary reason for the interest in an aerodynamic model of the X8. Some examples of its use is autonomous net landing[20], design of a model based longitudinal controller based on system identification[21] , platform for different camera-based experiments [22]–[26]. Reference [27] use the X8 in experiments with vision based roll angle determination, [28] installed fuel cells, while [29] use it in experiments on communication-aware path planning.

Validating CFD results with wind tunnel measurements is nothing new. Thus the focus of this paper is the lessons learned in the process, and the presentation of the X8 aerodynamic model. The paper is organized into 7 section. Section II presents the structure of the aerodynamic model that lays the foundation for the identification process. The wind tunnel experiments, with its challenges, the design and the subsequent parameter estimation, is introduced in Section III, while the numerical modeling is presented in Section IV. Sections V to VI states and discusses the results from the wind tunnel and numerical calculations, upon which the concluding remarks of Section VII are drawn.

II. Aerodynamic model structure

Through Newtons laws of motion, the general six degrees-of-freedom equations of motion in Eq. (1) relate the force F and moment M to linear and angular motion of a rigid body of mass m and with an inertia matrix $\boldsymbol{I}$.

$$\begin{aligned} m\dot{\boldsymbol{V}} + \boldsymbol{\omega} \times m\boldsymbol{V} &= \boldsymbol{F} \\ \boldsymbol{I}\dot{\boldsymbol{\omega}} + \boldsymbol{\omega} \times \boldsymbol{I}\boldsymbol{V} &= \boldsymbol{M} \end{aligned} \tag{1}$$

Here, $\boldsymbol{V} = [u, v, w]$ are the velocities along the body x, y, z-axes, while $\boldsymbol{\omega} = [p, q, r]$ are the angular rates about the same axes. For a UAV, the force is often split into gravity, $\boldsymbol{F}_g$, thrust, $\boldsymbol{F}_t$ and aerodynamic forces, $\boldsymbol{F}_a$, as seen in Eq. (2). The same is true for the moment $\boldsymbol{M}$, but it is assumed to act around the center of gravity, thus being independent of gravity.

$$\begin{aligned} \boldsymbol{F} &= \boldsymbol{F}_a + \boldsymbol{F}_g + \boldsymbol{F}_t \\ \boldsymbol{M} &= \boldsymbol{M}_a + \boldsymbol{M}_t \end{aligned} \tag{2}$$

As propulsion and gravitational forces and moments are not considered in this paper, see [19] for a reference on how they can be modeled.

The aerodynamic forces are modeled in the wind frame, and are rotated into the body frame, see Fig. 1.

$$\boldsymbol{F}_a = \begin{bmatrix} F_x \\ F_y \\ F_z \end{bmatrix} = \mathbf{R}_w^b(\alpha, \beta) \begin{bmatrix} -D \\ Y \\ -L \end{bmatrix}, \tag{3}$$

where, D, Y and L are the aerodynamic drag-, side- and lift forces, acting along the negative x, positive y and negative z axes of the wind frame[19], and where

$$\mathbf{R}_w^b(\alpha, \beta) = \begin{bmatrix} \cos(\alpha)\cos(\beta) & \cos(\alpha)\sin(\beta) & -\sin(\alpha) \\ -\sin(\beta) & \cos(\beta) & 0 \\ \cos(\beta)\sin(\alpha) & \sin(\alpha)\sin(\beta) & \cos(\alpha) \end{bmatrix}, \tag{4}$$

is the rotation matrix from wind- to body frame. Here, $\alpha = \tan^{-1}(\frac{u-u_w}{w-w_w})$ and $\beta = \sin^{-1}(\frac{v-v_w}{Va})$ is the angle-of-attack and the side-slip-angle, respectively.

A general model of the aerodynamic forces and moments acting on a fixed-wing UAV is given in Eq. (5). The aerodynamic moments l, m, n are about the x, y, z axes of the body frame. The drag-, side- and lift foces acting on an object are typically modeled in terms of the dimensionless functions C_D, C_Y and C_L. Similarly, the roll-, pitch- and yaw moments, are modeled in terms of C_l, C_m and C_n, as

well as the characteristic lengths b and c that represent wing span and mean aerodynamic chord.

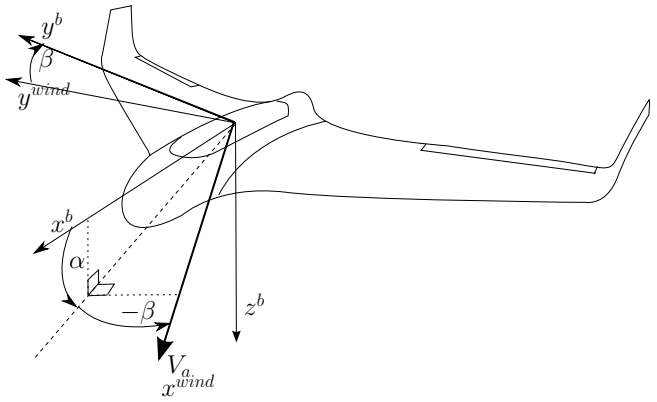

Fig. 1: Wind and body axes

$$\begin{bmatrix} D \\ Y \\ L \end{bmatrix} = \frac{1}{2}\rho V_a^2 S \begin{bmatrix} C_D(\alpha,\beta,p,q,r,\delta_a,\delta_e,\delta_r) \\ C_Y(\alpha,\beta,p,q,r,\delta_a,\delta_e,\delta_r) \\ C_L(\alpha,\beta,p,q,r,\delta_a,\delta_e,\delta_r) \end{bmatrix}$$
$$\begin{bmatrix} l \\ m \\ n \end{bmatrix} = \frac{1}{2}\rho V_a^2 S \begin{bmatrix} bC_l(\alpha,\beta,p,q,r,\delta_a,\delta_e,\delta_r) \\ cC_m(\alpha,\beta,p,q,r,\delta_a,\delta_e,\delta_r) \\ bC_n(\alpha,\beta,p,q,r,\delta_a,\delta_e,\delta_r) \end{bmatrix} \quad (5)$$

Here, $[u_w, v_w, w_w]$ are the wind speeds along the body x, y, z-axis, and $\delta_a, \delta_e, \delta_r$ are the control inputs to the aileron, elevator and rudder. S is the area of the wing, ρ is the air density and V_a is the airspeed. Equation (5) already makes the common assumptions that Froude-, Mach-, Strouhal- and Reynolds number effects are small, and that the mass and inertia of the aircraft is dominating that of the surrounding air[3].

A common, further simplification for flight with small angles-of-attack is to assume that lift- and pitch moment coefficients are linear in α, q and δ_e, and independent of β, p, r, δ_r and δ_a. The roll- and yaw coefficients, on the other hand, are independent of α, q and δ_e, and linear in β, p, r, δ_r and δ_a. However, due to the drag force's quadratic nature in α, a linear model in drag is often deemed unfit [3].

The above decoupling between the lateral and longitudinal axes is questionable, but very common[30]. One coupling term for flight at low angles-of-attack is the drag forces dependence on side-slip-angle. Due to symmetry about the xz-plane, drag is an even function in the side-slip-angle.

In summary, the force and moment coefficients are expressed as in Eq. (6). This paper assumes metric units in the aerodynamic model. Specifically, angles, including control surface deflections, and angular rates are given in radians and radians per second. However, degrees are used for plotting.

III. Wind tunnel testing

The accuracy of the data from a wind tunnel depends on the accuracy of the mass balance. Since this accuracy usually is given as a percentage of the nominal load for the mass balance, the nominal load should reflect the expected loads in the experiment.

An inherent problem with wind tunnel testing of small UAVs is that they operate at lower Reynolds numbers (Re)[1] than larger aircraft, for which most wind tunnels are designed. This means that the forces exerted by UAVs on the mass balance are very small. To maximize the signal-to-noise ratio of the measured forces in the experiment, there are two obvious solutions, each with its own weakness. The first option is to decrease the noise by utilizing a mass balance designed for measuring small forces. Such mass balances generally have a smaller range and are more expensive. The other solution is to maximize the forces exerted by the UAV on the mass balance, such that the mass balance accuracy becomes negligible in comparison. This translates into performing the tests at higher Reynolds numbers, since there is a direct relationship between force and Reynolds number. The Reynolds number can be increased by using a larger model of the UAV, by decreasing the viscosity, or by increasing the airspeed, the latter being the most practical. A drawback with this approach is the larger structural load it will put on the UAV. In addition to potentially damaging the UAV structurally, the deflection of the control surfaces will change if the servos can not hold the larger moment generated by the increased airspeed. Also, the Reynolds numbers should be representable for actual flight conditions.

The problem with low accuracy of the mass balance is particularly pronounced in drag, as these forces are typically one order of magnitude lower than the lift forces. This well known difficulty has been addressed in e.g. [31] and [32]. One way to increase accuracy is to use a wind rake to measure the airspeed reduction downstream of the wind, determine the loss of energy, and thereby the drag. While being accurate, this method suffers from the curse of dimensionality as it requires spatial sampling of the airspeed, making it less feasible for streams in three dimensions.

A. Test setup

The wind tunnel testing presented in this section were conducted at the Czech Aerospace Research Center (VZLU) in Prague, Czech Republic. In order to mount the UAV into the wind tunnel, a hole was made in the rear of the fuselage so that the mass balance could be firmly attached to the inside. This internally mounted multi-component strain-gauge mass balance is used to measure the forces and moments acting on the UAV. Table I gives its nominal forces/moments and accuracy, along with basic specifications for the wind tunnel[2]. The mass balance is further attached to a vertical rod, as seen in Fig. 2. This rod can be rotated longitudinally and laterally, to change the angle-of-attack and side-slip-angle respectively. Before each test, the mass balance was calibrated for the current location of the center of gravity in the UAV, so that contributions from gravity on the measured moments can be corrected for. This was

[1]The nondimensional Reynolds number is defined as $\mathrm{Re} = \frac{V_a L}{\nu}$, where L is the characteristic length of the UAV, i.e. the mean aerodynamic chord, while ν is the kinematic viscosity of air.

[2]For more information about the wind tunnel in question, see also `http://www.vzlu.cz/en/low-speed-wind-tunnels-c73.html`.

$$\begin{bmatrix} C_D \\ C_Y \\ C_L \end{bmatrix} = \begin{bmatrix} C_{D_0} + C_{D_{\alpha 1}}\alpha + C_{D_{\alpha 2}}\alpha^2 + C_{D_{\delta_e}}\delta_e^2 + C_{D_q}\frac{c}{2V_a}q + C_{D_{\beta 2}}\beta^2 + C_{D_\beta}\beta \\ C_{Y_0} + C_{Y_\beta}\beta + C_{Y_p}\frac{b}{2V_a}p + C_{Y_r}\frac{b}{2V_a}r + C_{Y_{\delta_a}}\delta_a + C_{Y_{\delta_r}}\delta_r \\ C_{L_0} + C_{L_\alpha}\alpha + C_{L_q}\frac{c}{2V_a}q + C_{L_{\delta_e}}\delta_e \end{bmatrix}$$
$$\begin{bmatrix} C_l \\ C_m \\ C_n \end{bmatrix} = \begin{bmatrix} (C_{l_0} + C_{l_\beta}\beta + C_{l_p}\frac{b}{2V_a}p + C_{l_r}\frac{b}{2V_a}r + C_{l_{\delta_a}}\delta_a + C_{l_{\delta_r}}\delta_r) \\ C_{m_0} + C_{m_\alpha}\alpha + C_{m_q}\frac{b}{2V_a}q + C_{m_{\delta_e}}\delta_e \\ (C_{n_0} + C_{n_\beta}\beta + C_{n_p}\frac{b}{2V_a}p + C_{n_r}\frac{b}{2V_a}r + C_{n_{\delta_a}}\delta_a + C_{n_{\delta_r}}\delta_r) \end{bmatrix} \quad (6)$$

done by sweeping through the range of angles-of-attack or side-slip-angles while the air is not flowing, to calculate the moment contributions from gravity at each angle.

TABLE I: Wind tunnel specifications

Wind tunnel type	Closed
Test section	Open
Test section diameter	3 m
Test section length	3 m
Maximum velocity	90 m/s
Max. deviation between local and mean velocity	<0.5 %
Characteristic turbulence intensity	0.3
Nominal X Force	825 N ±0.5%
Nominal Y Force	825 N ±0.5%
Nominal Z Force	2500 N ±0.5%
Nominal Mx Moment	150 Nm ±0.5%
Nominal My Moment	175 Nm ±0.5%
Nominal Mz Moment	150 Nm ±0.5%

To be able to adjust the control surfaces during the experiments, the UAV was equipped with a reduced version of its avionics [33] consisting of two Hitec HS-5085MG digital servos, a BeagleBone Black single board computer, and a small WiFi router for communication with the control room. As servos rely on a PWM command, not a deflection angle, a program was made to translate the commanded angle to a PWM signal, based on curve fitting of empirical data.

A challenge with the servos is that the angular output of the RC servos typically found in small UAVs are not consistent when approaching the same angle from different sides; commanding an angle of 0° yields a slightly different result when commanded from e.g. 10° than when commanded from e.g. -10°, due to the hysteresis of the servo motor and gear. This is mitigated by always commanding the servo to go to the maximum PWM value before a new angle is commanded.

B. Design of experiments

In addition to mitigating the challenges mentioned in the start of Section III, the experiments were designed to be as efficient as possible. The experiments focused on making a good model for the flight envelope that is used the most. This translates into focusing on the quality of the model around $\alpha = \beta = \delta_a = \delta_e = \delta_r = 0$ and Re corresponding to cruise speed, and spending time on verifying these data rather than exploring new regimes of the flight envelope.

The Reynolds numbers for the X8 during cruise speed of $18\,\mathrm{m/s}$ vary in the range $400\,000$ to $500\,000$ when the air temperature changes from $-10\,^\circ\mathrm{C}$ to $30\,^\circ\mathrm{C}$, which are both within the operational limits of the X8. Therefore, both these Reynolds numbers where included in the experiments.

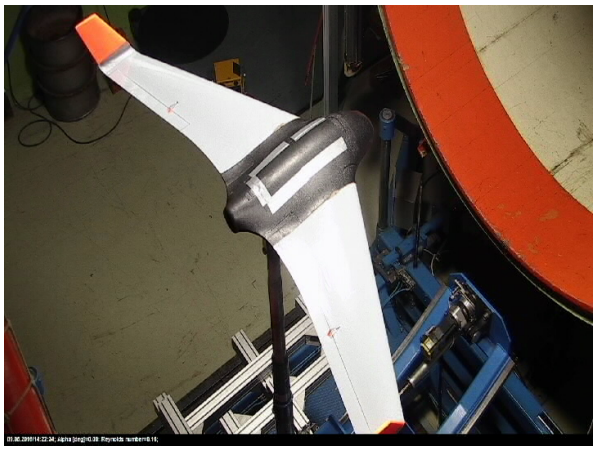

Fig. 2: The Skywalker X8 mounted in the wind tunnel

In order to simplify the testing process, and drastically reduce the number of tests that need to be performed, a common assumption is that the longitudinal and lateral dynamics are decoupled. The following sections go into detail on the tests for the different axes.

1) Longitudinal dynamics: The longitudinal tests focused on expressing the lift, drag and pitch moment as functions of angle-of-attack and elevator deflection, and assumed linearity in the angle-of-attack up to the stall of the wing. The tests are performed by sweeping through the different angles-of-attack for different Reynolds numbers and elevator deflections, while keeping the aileron and side-slip-angle constant at zero, see Table II.

TABLE II: Longitudinal axes tests for the X8

Test #	$\alpha[^\circ]$	Re	δ_e [°]
1	$[-5, 15]$	$\{0.4, 0.5\} \times 10^6$	0
2	$[-5, 15]$	$\{0.4, 0.5\} \times 10^6$	-20
3	$[-5, 15]$	$\{0.4, 0.5\} \times 10^6$	-10
4	$[-5, 15]$	$\{0.4, 0.5\} \times 10^6$	-5
5	$[-5, 15]$	$\{0.4, 0.5\} \times 10^6$	20
6	$[-5, 15]$	$\{0.4, 0.5\} \times 10^6$	10
7	$[-5, 15]$	$\{0.4, 0.5\} \times 10^6$	55

2) Lateral dynamics: The lateral tests focused on expressing the side force, roll moment and yaw moment as functions of side-slip-angle, aileron deflection, and assumed linearity in side-slip-angle up to the stall of the winglets. The tests were performed by sweeping through the different side-slip-

angles for different Reynolds numbers and control surface deflections, while keeping the angle-of-attack constant at zero. In the interest of time, symmetry around the body x-axis was assumed. The lateral tests performed on the X8 are listed in Table III.

TABLE III: Lateral axes tests for the X8

Test #	$\beta[^\circ]$	Re	δ_a $[^\circ]$
1	$[-15, 15]$	$\{0.25, 0.5\} \times 10^6$	0
2	$[-15, 15]$	$\{0.25, 0.5\} \times 10^6$	20
3	$[-15, 15]$	$\{0.25, 0.5\} \times 10^6$	10

3) Coupled dynamics: The questionable assumption that longitudinal and lateral dynamics are decoupled can be necessary in the interest of time efficiency. If using a 6 DOF mass balance, the drag component from varying side-slip-angle is already found from the lateral tests, so the inclusion of this coupling term does not require any more time. Other important couplings between the lateral and longitudinal dynamics can vary from airframe to airframe, and a decision on what coupled dynamics should be included in the model relies on the UAV design and experience from flight tests or simulations. Other coupling terms, like the angle-of-attack dependency of the roll damping coefficient C_{l_p}, are not considered here since they are small and complicate the estimation procedure.

C. Parameter estimation

Once the data from the wind tunnel testing were recorded, they were fit to the model given by Eq. (6), through reformulation into a linear regression model of the form $y_i = \boldsymbol{\varphi}_i^T \boldsymbol{\Theta} + \epsilon_i$. Here, the measured variable y_i corresponds to the i'th quasi-measurement[3] of an aerodynamic coefficient $C_* \left(\alpha, \beta, p, q, r, \delta_a, \delta_e, \delta_r\right)$, $\boldsymbol{\varphi}_i$ is a vector of explanatory variables, $\boldsymbol{\Theta}$ is a parameter vector of the coefficient to be determined, and ϵ_i is an error term that accounts for the measurement noise as well as any unmodeled effects.

The goal of the parameter estimation is to find the value of the coefficients $\boldsymbol{\Theta}$ that explain the measurements y_i, given the explanatory variables $\boldsymbol{\varphi}_i$, in a way that minimize the error ϵ_i. This can be achieved by minimizing the squared error between the measurement y_i and the estimate $\hat{y}_i = \boldsymbol{\varphi}_i^T \boldsymbol{\Theta}$, known as the least squares problem:

$$\begin{aligned} \hat{\boldsymbol{\Theta}} &= \arg \min_{\boldsymbol{\Theta} \in \mathcal{R}^d} V(\boldsymbol{\varphi}, \boldsymbol{\Theta}) \\ &= \arg \min_{\boldsymbol{\Theta} \in \mathcal{R}^d} \frac{1}{2N} \sum_{i=1}^{N} \left(y_i - \boldsymbol{\varphi}_i^T \boldsymbol{\Theta}\right)^2, \end{aligned} \tag{7}$$

where d is the dimension of the parameter vector, while N is the number of measurements. Table IV lists the explanatory variables and coefficients for the model Eq. (6). For the tests with the X8, the angular rates p, q, and r where zero, due to the limitations of the wind tunnel facility.

[3]The aerodynamic coefficients are considered *quasi*-measurements since they are not directly measured, but derived from the measurements of the forces and moments acting on the mass balance in the body frame.

There are many ways to find a solution to the least squares parameter estimation problem Eq. (7). See e.g. [3] for an in-depth explanation on parameter estimation.

The parameter estimation procedure is greatly simplified by using the MATLAB curve fitting toolbox[4].

IV. Numerical modelling

Numerical modelling was chosen to be performed with XFLR5 as it is an easy and fast tool to use. The code performs reasonably well for viscid 2D and with limitations also in 3D[34]. Generally, the biggest limitations are on the 3D methods, as the best results are obtained for thin surfaces at low angles of attack. The deviations increase as the aircraft geometry differs from an idealized 2D infinite wing. Also, flows with large rotational components (especially turbulence) cannot be captured accurately. However, XFLR5 can be used to support wind tunnel testing data and is here used to determine the stability coefficients which were not obtained experimentally.

To model a fixed-wing aircraft in XFLR5, knowledge of its geometry is required, in particular the shape of the airfoils that are used. Unfortunately, the airfoil of the X8 is unknown, even after comparing it to commonly used flying wing airfoils. However, the X8 geometry was found from an openly available 3D-scan of the Skywalker X8[5]. The 3D model is in a raw format meaning that the surface of the aircraft is uneven and shows erroneous artifacts. When extracting 2D cross sections to be used in the XFLR5 code, the 2D airfoils will be edgy and containing an uneven curvature which leads to unrealistic predictions of the pressure and velocity distribution. In order to minimize this effect, the 2D cross sections have been smoothed manually using XFLR5. First, the geometry is approximated with a spline. Second, the inverse foil design tool is used on the spline to generate a smooth pressure distribution on the surface. The resulting airfoil has good confidence that the mean chamber line have been captured correctly, which is affecting lift. The airfoil curvature however, is not well captured as the input data was too inaccurate. Airfoil curvature affects the resulting pressure gradients which are driving the boundary layer transition processes. These are responsible for the generation of drag and pitch forces. Hence, it is expected that the XFLR5 data will perform well for lift and poor for drag and pitch. The final step of the modeling in XFLR5 is to assemble the airfoils into a wing, and possibly add a fuselage. The X8 wing and fuselage was modeled as a blended wing, with no fuselage, since there is no clear distinction between the two.

XFLR5 can perform two types of analysis: a static analysis and a stability analysis[6]. The static analysis sweeps through a range of angle-of-attack or side-slip-angles for a range of Reynolds numbers, to generate polars that show how the

[4]https://www.mathworks.com/products/curvefitting.html

[5]The 3D-scan of the X8 can be found at `https://diydrones.com/profiles/blogs/x8-3d-scanning`

[6]The static and stability analyses are referred to as *Analysis* and *Stability Analysis* in XFLR5

TABLE IV: Explanatory variables and parameter vector for the different measurements

y	$\boldsymbol{\varphi}^T$	$\boldsymbol{\Theta}^T$
C_D	$[1, \alpha, \alpha^2, \frac{c}{2V_a}q, \beta^2, \beta, \delta_e^2]$	$[C_{D_0}, C_{D_{\alpha 1}}, C_{D_\alpha 2}, C_{D_q}, C_{D_{\beta 2}}, C_{D_\beta}, C_{D_{\delta_e}}]$
C_Y	$[1, \beta, \frac{b}{2V_a}p, \frac{b}{2V_a}r, \delta_a, \delta_r]$	$[C_{Y_0}, C_{Y_\beta}, C_{Y_p}, C_{Y_r}, C_{Y_{\delta_a}}, C_{Y_{\delta_r}}]$
C_L	$[1, \alpha, \frac{c}{2V_a}q, \delta_e]$	$[C_{L_0}, C_{L_\alpha}, C_{L_q}, C_{L_{\delta_e}}]$
C_l	$[1, \beta, \frac{b}{2V_a}p, \frac{b}{2V_a}r, \delta_a, \delta_r]$	$[C_{l_0}, C_{l_\beta}, C_{l_p}, C_{l_r}, C_{l_{\delta_a}}, C_{l_{\delta_r}}]$
C_m	$[1, \alpha, \frac{c}{2V_a}q, \delta_e]$	$[C_{m_0}, C_{m_\alpha}, C_{m_q}, C_{m_{\delta_e}}]$
C_n	$[1, \beta, \frac{b}{2V_a}p, \frac{b}{2V_a}r, \delta_a, \delta_r]$	$[C_{n_0}, C_{n_\beta}, C_{n_p}, C_{n_r}, C_{n_{\delta_a}}, C_{n_{\delta_r}}]$

forces and moments vary with angle-of-attack or side-slip-angle. The stability analysis calculates the damping terms and control input coefficients by approximating the partial derivatives of the aerodynamic forces and moments. The forward differentiation approximation is acheived by slightly perturbing the UAV by a slight change in attitude, velocity or control surface deflection, and noting how much the forces and moments change. A finite difference approximation is found by dividing this change in force/moment by the perturbation.

The data from the different XFLR5 analyses were then fit to the model Eq. (5), in a similar manner as the wind tunnel data.

V. Results

From the geometry of the 3D model of the Skywalker X8, the wingspan and mean aerodynamic chord were found to be $2.1\,\mathrm{m}$ and $35.7\,\mathrm{cm}$, respectively. This was used in the subsequent parameter identification, whose resulting aerodynamic coefficients are shown in Table V, along with the root mean square error (RMSE) and coefficient of determination (R^2) corresponding to the fitting of the wind tunnel data. The table also contains the data from the numerical analysis, both for comparison to the wind tunnel (WT) data and for complementing the wind tunnel data with stability coefficients. Figures 3a to 3f and Fig. 4 visualize the fit of the model along with the measured data from the wind tunnel, for all the six axes. The differences in the coefficient, for the same control surface deflection angle and angle-of-attack/side-slip-angle, comes from running the tests at different Reynolds numbers. As seen in Figs. 3a, 3c and 3e, the longitudinal fitting exclude data points with angle-of-attack of more than 12° and less than 0° to avoid the stall region.

The R^2-column shows that most of the coefficients from the wind tunnel experiment fit well with the data. The exception is the lateral drag, C_{β_2} and C_{β_1}, which likely comes from the large relative difference between the data for different Re, compared to the magnitude of the coefficient, as shown in Fig. 4. The fit did not improve for higher order polynomials.

Unfortunately, neither XFLR5 nor the wind tunnel testing is able to estimate the increase in drag from pitch rate, C_{D_q}.

VI. Discussion

The coefficients from XFLR5 and from the wind tunnel testing match reasonably well, with some exceptions.

TABLE V: Skywalker X8 aerodynamic coefficients

	WT	XFLR5	RMSE	R^2
C_{L_0}	0.0867	0.0477	0.0153	0.996
C_{L_α}	4.02	4.06	0.0153	0.996
$C_{L_{\delta_e}}$	0.278	0.7	0.0153	0.996
C_{L_q}	–	3.87	–	–
C_{D_0}	0.0197	0.0107	0.00262	0.982
$C_{D_\alpha 1}$	0.0791	−0.00955	0.00262	0.982
$C_{D_\alpha 2}$	1.06	1.1	0.00262	0.982
$C_{D_{\delta_e}}$	0.0633	0.0196	0.00262	0.982
$C_{D_{\beta_2}}$	0.148	0.115	0.00234	0.734
$C_{D_{\beta_1}}$	−0.00584	$-2.34E-19$	0.00234	0.734
C_{m_0}	0.0302	0.00439	0.00576	0.983
C_{m_α}	−0.126	−0.227	0.00576	0.983
$C_{m_{\delta_e}}$	−0.206	−0.325	0.00576	0.983
C_{m_q}	–	−1.3	–	–
C_{Y_0}	0.00316	$1.08E-08$	0.00326	0.991
C_{Y_β}	−0.224	−0.194	0.00326	0.991
$C_{Y_{\delta_a}}$	0.0433	0.0439	0.00326	0.991
C_{Y_p}	–	−0.137	–	–
C_{Y_r}	–	0.0839	–	–
C_{l_0}	0.00413	$1.29E-07$	0.00476	0.953
C_{l_β}	−0.0849	−0.0751	0.00476	0.953
$C_{l_{\delta_a}}$	0.12	0.202	0.00476	0.953
C_{l_p}	–	−0.404	–	–
C_{l_r}	–	0.0555	–	–
C_{n_0}	−0.000471	$1.51E-07$	0.000615	0.98
C_{n_β}	0.0283	0.0312	0.000615	0.98
$C_{n_{\delta_a}}$	−0.00339	−0.00628	0.000615	0.98
C_{n_p}	–	0.00437	–	–
C_{n_r}	–	−0.012	–	–

Figure 5 compares the angle of attack against the lift coefficient for all the models used. As expected, model and experiment show a good fit of the lift gradient. An constant offset of approximately $\alpha = 0.5^\circ$ of the XFLR5 and wind tunnel data is observable which might be related to an offset in angle of attack during the wind tunnel testing. This is reasonable as the definition of the zero angle in the wind tunnel was difficult to achieve.

Figure 6 displays the aircraft performance; lift versus drag. The drag values show significant deviation from the wind tunnel results. This was expected and can be attributed to the deviations from the real airfoil geometry as well as the code limitations of XFLR5. The numeric method under-predicts the drag by approximately 50% in the linear region, which is probably caused by the difficulty in predicting viscous effects. As the drag forces are not captured accurately by XFLR5 this means that the pitching moment will also be subject to the same error.

Furthermore, Figure 6 shows that the main difference in

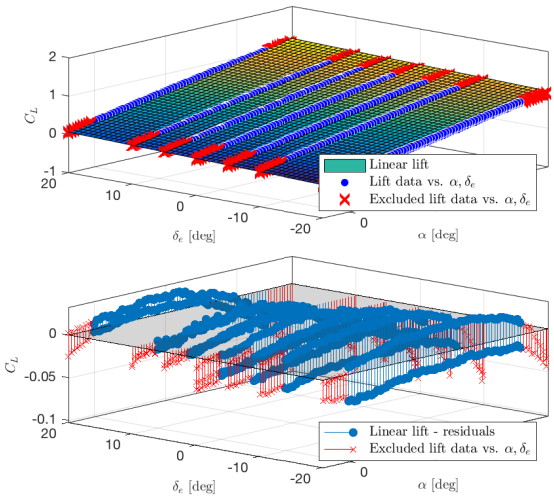

(a) Lift force coefficient fit

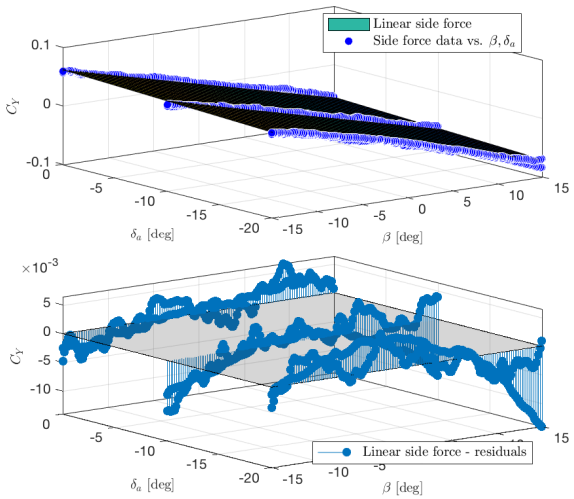

(b) Side force coefficient fit

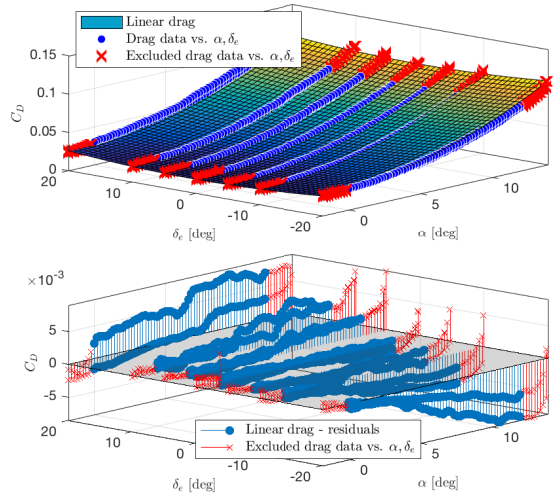

(c) Drag force coefficient fit

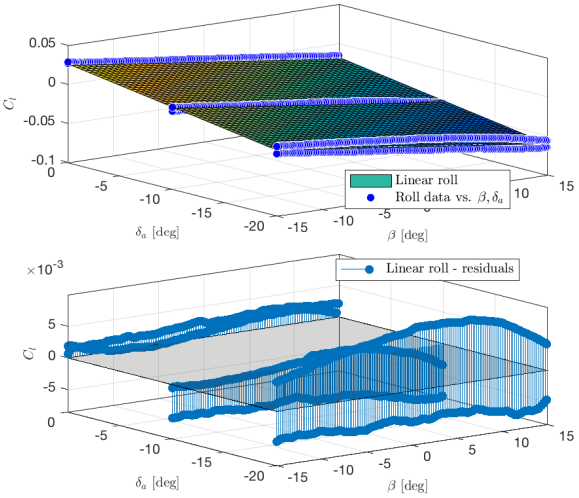

(d) Roll moment coefficient fit

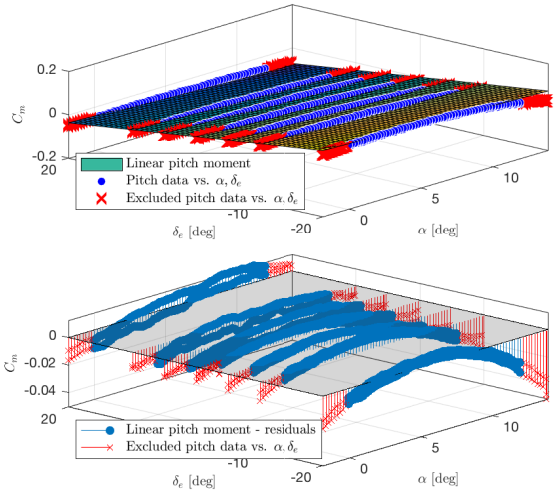

(e) Pitch moment coefficient fit

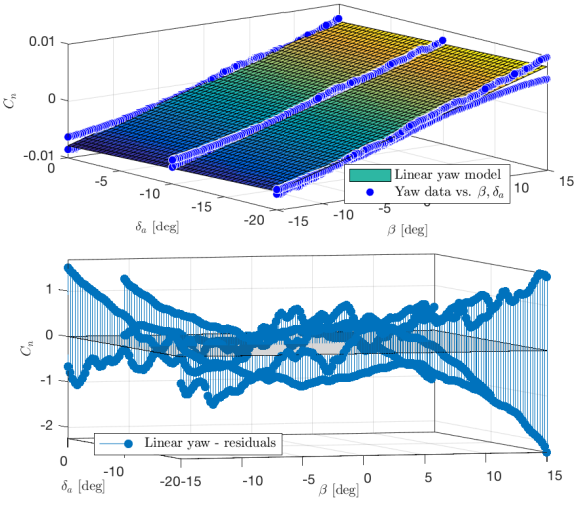

(f) Yaw moment coefficient fit

Fig. 3: Curve fit

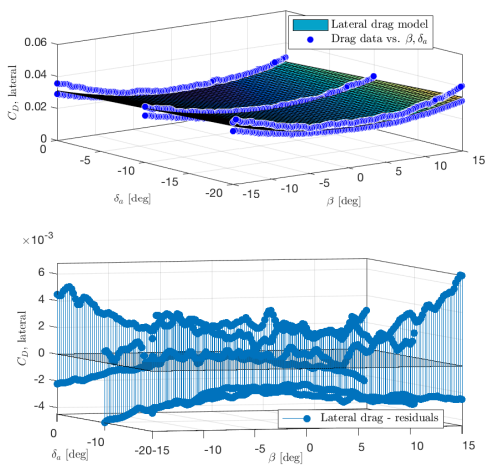

Fig. 4: Lateral drag

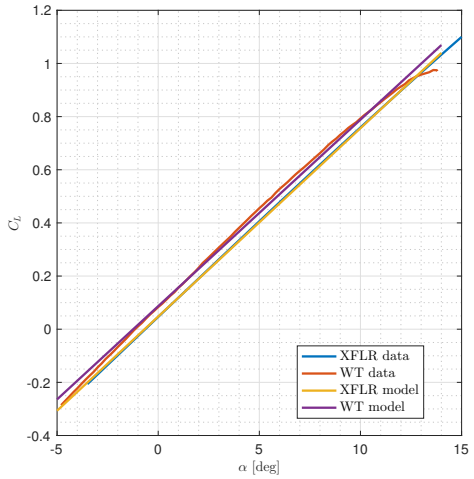

Fig. 5: Lift coefficient vs. angle-of-attack

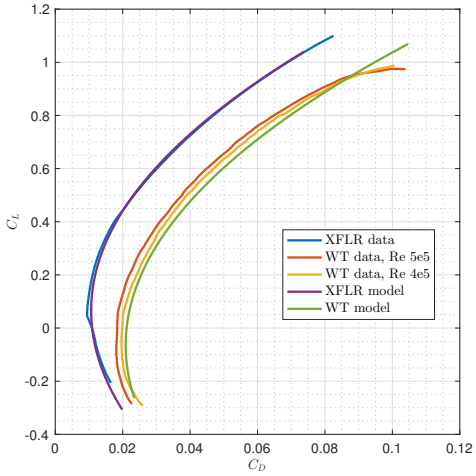

Fig. 6: Lift coefficient vs. drag coefficient

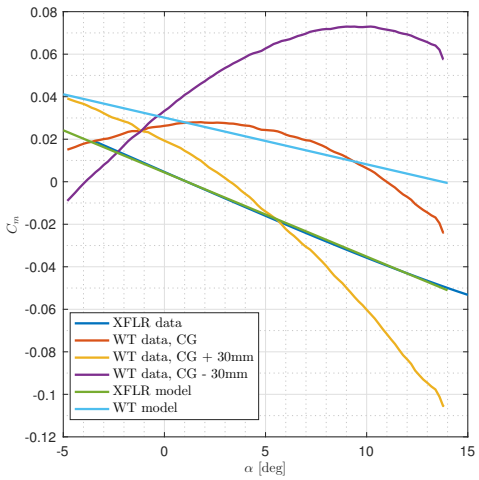

Fig. 7: Pitching moment coefficient vs. angle-of-attack

drag is a constant offset. This could come from the fact that the theoretical background of the methods in XFLR5 are based on inviscid flow, and use an ad-hoc method for viscous calculations. Another error source for the drag from XFLR5 could be the trailing edge of the fuselage. It has a blunt edge, which is an inherent problem with panel methods. In addition to the measurement errors, the precision of the wind tunnel data is also compromised by blockage effects in the wind tunnel, which has been accounted for by VZLU, and by its finite width. The wind tunnel is $0.9\,\mathrm{m}$ wider than the wing span of the UAV, so wing tips might be affected by the boundary layer outside the airflow in the open section of the wind tunnel. Among the longitudinal control derivatives, $C_{m_{\delta_e}}$ from the wind tunnel and from XFLR5 are in the same orders of magnitude. Consistent with XFLR5s over prediction of the aircraft performance, $C_{L_{\delta_e}}$ from XFLR5 is far larger, while drag, $C_{D_{\delta_e}}$, is smaller.

In the pitch moment, Fig. 7 reveals larger differences than one would expect from Table V. The wind tunnel data is very nonlinear in angle-of-attack, and does not fit well with neither the XFLR5- nor the wind tunnel models. It can also be seen that the wind tunnel data indicate instability for $\alpha < 2°$. Since the X8 is a flying wing, $C_m(\alpha)$ is small, and very sensitive to changes in the center of gravity, so the instability can come from using wrong center of gravity. Currently, the location of the center of gravity is $44.0\,\mathrm{cm}$ behind the nose of the UAV, and is based on experience from flights, but as shown in Fig. 7, a slight shift of the center of gravity $30\,\mathrm{mm}$ to the front yields a large stability margin in the pitching moment. It is also shown that the zero moment for the CG-centered curve is at about $\alpha = 11°$, which is unrealistically high. The curve referenced $30\,\mathrm{mm}$ in front of the center of gravity yields zero pitching moment at $\alpha = 3.25°$, which is more in line with experience from flight testing. There are some differences in C_{Y_0}, C_{l_0} and C_{n_0}, but these likely come from misalignment in the wind tunnel testing, as these

coefficients should be zero for an airframe with symmetry about the xz-plane.

With these differences, it is difficult to conclude on the confidence in the stability coefficients from XFLR5, and this matter should be investigated further in flight test validation. However, it is clear that XFLR5 easily and quickly gives reasonable data that can be valuable for initial estimates of static aerodynamic coefficients. Estimation of stability coefficients in a wind tunnel require more advanced equipment, in the form of a rotary balance, and considerably more time.

For estimation and control purposes, wind gusts are considered model disturbances. Small UAVs are likely to encounter large wind gusts disturbances, that are difficult to measure. This indicates that regardless of the precision of the aerodynamic model, considerable amounts of noise will degrade the performance of the estimation or control algorithm that utilize the model.

Further, it is apparent from the residual in Figs. 3a to 3f that the averaging of the coefficients over the different Reynolds numbers yields a good fit in the flight regime on average, as intended, but the precision could have improved by only fitting the model to the data from one Reynolds number. This is also true for the fitting to the control surface deflections. Figure 6 shows that the model differs from the measurements for both Reynolds numbers, when $\delta_e = 0$. However, the least squares estimation has ensured that the model reduces the estimation error over all Re and δ_e. In order to improve the fit at $\delta_e = 0$, weighted least squares could have been used instead.

Through the work with these tests, it has become apparent that wind tunnels are not ground truth, as there is a lot of measurement errors, especially in drag. This comes from the relative low accuracy of mass balances designed for larger forces than what is typically exerted by the air on small UAVs. Further, the importance of checking the measurements was demonstrated; the experiments presented in this paper where performed twice, since the data from the first test was found to be corrupted by a faulty axis on the mass balance. Another costly lesson learned is that wings break when exposed to large airspeeds at large side-slip-angles. Considerable amounts of time can be saved by optimizing the test schedule, depending on the test facility. At the VZLU facilities, the angle-of-attack can be adjusted very easily. Adjusting the Reynolds number, i.e. the airspeed, takes more time since the flow has to stabilize. Adjusting the control surfaces is by far the more time consuming, since the center of gravity changes slightly with the deflection. Therefore, the model has to be tared again, by calculating the contributions from gravity at each angle-of-attack or side-slip-angle.

Other topics for future work include replacing XFLR5 with a Navier-Stokes-based CFD method to estimate the stability data with higher accuracy, integrating the presented model into the software-in-the-loop framework for ArduPlane, extending the model into the high angle-of-attack region, and adapting the model to icy conditions. The model is available for download[7], and will be updated with the results from future work.

VII. Conclusion

A mathematical model is always going to be an approximation of the physical world. This paper has presented considerations that are important to make, both in the experiment design and in the analysis of the data, in order to make the model as close a representation as possible, using numerical modeling backed by wind tunnel testing. The case study of the Skywalker X8 fixed-wing UAV indicate a reasonable match between the numerical results and the wind tunnel, particularly in lift, but show some discrepancies that needs further investigation through validation with flight data. Notably, the drag is under-predicted by the numerical modeling, and the sensitivity to center of gravity is reflected in the pitch moment from the wind tunnel testing. Also, the stability coefficients from the numerical modeling needs validation with real flight data, as they were not tested in the wind tunnel. To promote the use of the X8 model presented in this paper, it has been made publicly available for download.

Acknowledgements

The authors would like to thank Petr Vrchota and Robert Kulhánek at VZLU for invaluable guidance in the experiment design and in performing the wind tunnel tests. We would also like to thank Anthony Hovenburg and John Martin Kleven Godø at NTNU for discussions regarding the experiment design and in the data analysis.

References

[1] S. H. Mathisen, K. Gryte, T. I. Fossen, and T. A. Johansen, "Non-linear model predictive control for longitudinal and lateral guidance of a small fixed-wing uav in precision deep stall landing," in *AIAA SciTech*, 2016.

[2] K. T. Borup, T. I. Fossen, and T. A. Johansen, "A nonlinear model-based wind velocity observer for unmanned aerial vehicles," *IFAC-PapersOnLine*, vol. 49, no. 18, pp. 276–283, 2016.

[3] V. Klein and E. A. Morelli, *Aircraft system identification: Theory and practice*. American Institute of Aeronautics and Astronautics Reston, Va, USA, 2006.

[4] R. Jategaonkar, *Flight vehicle system identification: A time domain methodology*. Reston, VA, USA: AIAA, 2006, vol. 216.

[5] J. Blazek, *Computational fluid dynamics: Principles and applications*. Butterworth-Heinemann, 2015.

[6] M. Drela and H. Youngren, *Xfoil manual*, `http://web.mit.edu/aeroutil_v1.0/xfoil_doc.txt`, Accessed: 11.12.2014, 2001.

[7] Flight Level Engineering, *Surfaces aircraft design CFD software, web page*, http://www.flightlevelengineering.com/surfaces, Accessed 21.02.17.

[7] See `https://github.com/krisgry/x8`

[8] A. Deperrois, *XFLR5 analysis of foils and wings operating at low reynolds numbers*, http://sourceforge.net/projects/xflr5/files/Guidelines.pdf/download, 2013.

[9] W. H. Mason, *Software for aerodynamics and aircraft design*, Accessed 21.02.2017. [Online]. Available: http://www.dept.aoe.vt.edu/~mason/Mason_f/MRsoft.html.

[10] J. Katz and A. Plotkin, *Low-speed aerodynamics*. Cambridge university press, 2001, vol. 13.

[11] J. Krøgenes, L. Brandrud, R. Hann, J. Bartl, T. Bracchi, and L. Sætran, "Aerodynamic performance of the nrel s826 airfoil in icing conditions," *Wind Energy Science Discussions*, vol. 2017, pp. 1–17, 2017. [Online]. Available: https://www.wind-energ-sci-discuss.net/wes-2017-39/.

[12] K. Cunningham, D. Cox, D. Murri, and S. Riddick, "A piloted evaluation of damage accommodating flight control using a remotely piloted vehicle," in *AIAA Guidance, Navigation, and Control Conference*, 2011, p. 6451. [Online]. Available: https://ntrs.nasa.gov/archive/nasa/casi.ntrs.nasa.gov/20110014794.pdf.

[13] L. T. Nguyen, M. E. Ogburn, W. P. Gilbert, K. S. Kibler, P. W. Brown, and P. L. Deal, "Simulator study of stall/post-stall characteristics of a fighter airplane with relaxed longitudinal static stability.[f-16]," 1979.

[14] R. S. Russel, *Non-linear f-16 simulation using simulink and matlab*, Version 1.0, Jun. 2003. [Online]. Available: https://www.aem.umn.edu/people/faculty/balas/darpa_sec/software/F16Manual.pdf.

[15] N. M. Jodeh, "Development of autonomous unmanned aerial vehicle research platform: modeling, simulation, and flight testing," PhD thesis, Air force institute of technology, 2006.

[16] ArduPilot Development Team, *Ardupilot*, http://ardupilot.org, 2009–2018.

[17] G. Platanitis and S. Shkarayev, "Integration of an autopilot for a micro air vehicle," in *Infotech@Aerospace*, American Institute of Aeronautics and Astronautics (AIAA), Sep. 2005, p. 7066.

[18] DARcorporation, *Advanced aircraft analysis*, http://www.darcorp.com/Software/AAA/, Accessed 10.02.2018.

[19] R. W. Beard and T. W. McLain, *Small Unmanned Aircraft*. Princeton University Press, 2012.

[20] R. Skulstad, C. Syversen, M. Merz, N. Sokolova, T. Fossen, and T. Johansen, "Autonomous net recovery of fixed-wing uav with single-frequency carrier-phase differential gnss," *Aerospace and Electronic Systems Magazine, IEEE*, vol. 30, no. 5, pp. 18–27, 2015.

[21] J. Smith, J. Su, C. Liu, and W.-H. Chen, "Disturbance observer based control with anti-windup applied to a small fixed wing uav for disturbance rejection," *Journal of Intelligent & Robotic Systems*, vol. 88, no. 2-4, pp. 329–346, 2017.

[22] J. C. Ryan, A. L. Hubbard, J. E. Box, J. Todd, P. Christoffersen, J. R. Carr, T. O. Holt, and N. A. Snooke, "Uav photogrammetry and structure from motion to assess calving dynamics at store glacier, a large outlet draining the greenland ice sheet," 2015.

[23] A. S. Ferreira, J. Pinto, P. Dias, and J. B. de Sousa, "The lsts software toolchain for persistent maritime operations applied through vehicular ad-hoc networks," in *Unmanned Aircraft Systems (ICUAS), 2017 International Conference on*, IEEE, 2017, pp. 609–616.

[24] M. Faria, J. Pinto, F. Py, J. Fortuna, H. Dias, R. Martins, F. Leira, T. A. Johansen, J. Sousa, and K. Rajan, "Coordinating uavs and auvs for oceanographic field experiments: Challenges and lessons learned," in *Robotics and Automation (ICRA), 2014 IEEE International Conference on*, IEEE, 2014, pp. 6606–6611.

[25] J. Fortuna, F. Ferreira, R. Gomes, S. Ferreira, and J. Sousa, "Using low cost open source uavs for marine wild life monitoring-field report," *IFAC Proceedings Volumes*, vol. 46, no. 30, pp. 291–295, 2013.

[26] H. Tømmervik, S.-R. Karlsen, L. Nilsen, B. Johansen, R. Storvold, A. Zmarz, P. S. Beck, K. A. Høgda, S. Goetz, T. Park, *et al.*, "Use of unmanned aircraft systems (uas) in a multi-scale vegetation index study of arctic plant communities in adventdalen on svalbard," 2014.

[27] F. Gavilan, M. R. Arahal, and C. Ierardi, "Image deblurring in roll angle estimation for vision enhanced aav control," *IFAC-PapersOnLine*, vol. 48, no. 9, pp. 31–36, 2015.

[28] A. D. Meadowcroft, S. Howroyd, K. Kendall, and M. Kendall, "Testing micro-tubular SOFCs in unmanned air vehicles (UAVs)," *ECS Transactions*, vol. 57, no. 1, pp. 451–457, 2013.

[29] M. Stachura and E. Frew, "Communication-aware information-gathering experiments with an unmanned aircraft system," *Journal of Field Robotics*, vol. 34, no. 4, pp. 736–756, 2017.

[30] R. F. Stengel, *Flight Dynamics*. Princeton University Press, 2004.

[31] S. C. Smith, "A computational and experimental study of nonlinear aspects of induced drag," 1996.

[32] S. F. Hoerner, *Fluid-dynamic drag: Practical information on aerodynamic drag and hydrodynamic resistance*. Hoerner Fluid Dynamics Midland Park, NJ, 1965.

[33] A. Zolich, T. A. Johansen, K. Cisek, and K. Klausen, "Unmanned aerial system architecture for maritime missions. design & hardware description," in *Research, Education and Development of Unmanned Aerial Systems (RED-UAS), 2015 Workshop on*, IEEE, 2015, pp. 342–350.

[34] A. Deperrois, *About XFLR5 calculations and experimental measurements*, Accessed 15.09.2014. [Online]. Available: http://www.xflr5.com/docs/Results_vs_Prediction.pdf.